Nanoscale

www.rsc.org/nanoscale

Volume 3 | Number 2 | February 2011 | Pages 317–752

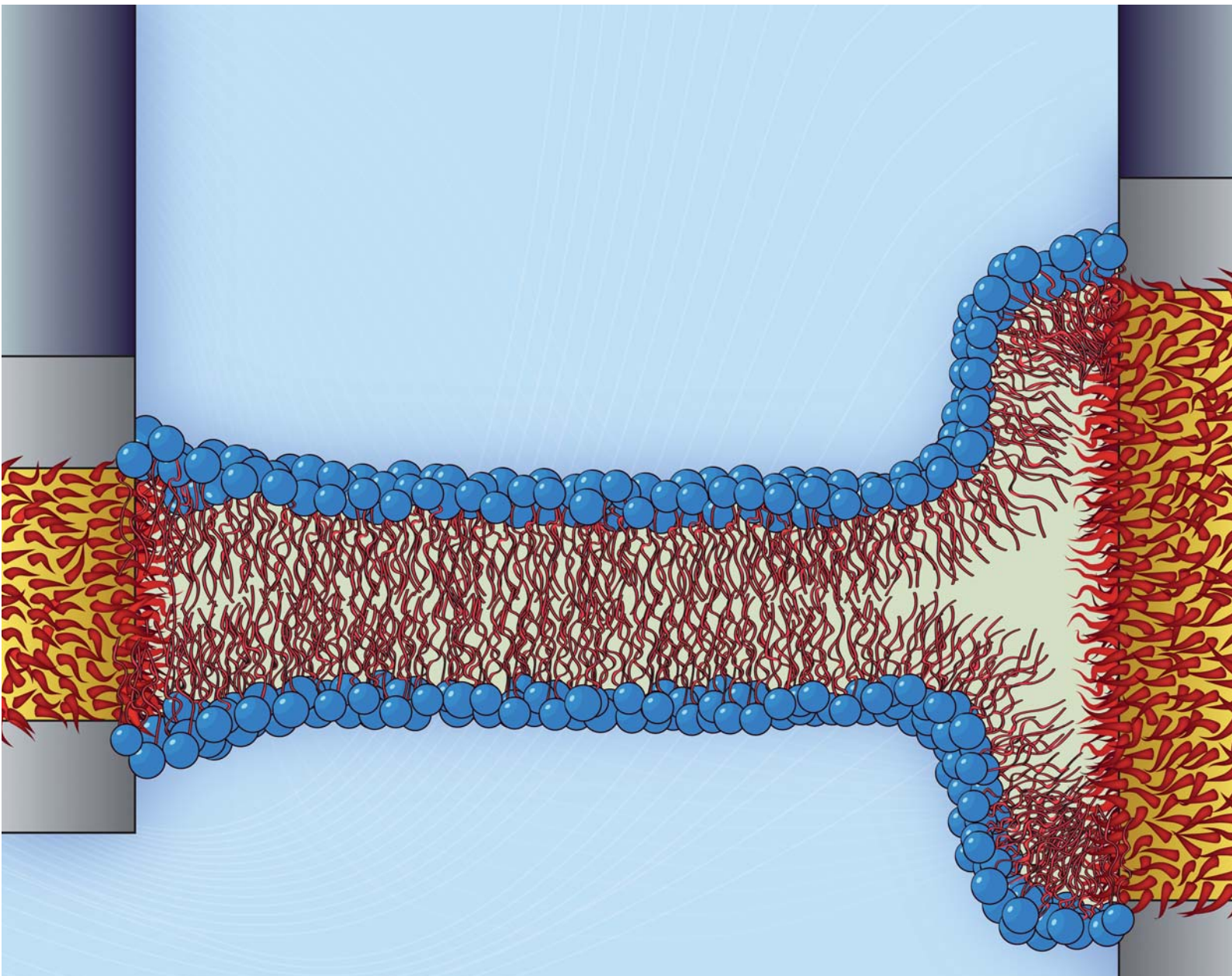

Includes a collection of articles on surface nanotechnology for biological applications

ISSN 2040-3364

RSC Publishing

RESEARCH ARTICLE
Melosh *et al.*
Nanoscale patterning controls inorganic-membrane interface structure

2040-3364(2011)3:2;1-Q

Nanoscale patterning controls inorganic–membrane interface structure†

Benjamin D. Almquist,[a] Piyush Verma,[a] Wei Cai[b] and Nicholas A. Melosh*[a]

Received 8th July 2010, Accepted 26th August 2010
DOI: 10.1039/c0nr00486c

Published on 07 October 2010 on http://pubs.rsc.org | doi:10.1039/C0NR00486C
Downloaded on 17 February 2011

The ability to non-destructively integrate inorganic structures into or through biological membranes is essential to realizing full bio-inorganic integration, including arrayed on-chip patch-clamps, drug delivery, and biosensors. Here we explore the role of nanoscale patterning on the strength of biomembrane–inorganic interfaces. AFM measurements show that inorganic probes functionalized with hydrophobic bands with thicknesses complimentary to the hydrophobic lipid bilayer core exhibit strong attachment in the bilayer. As hydrophobic band thickness increases to 2–3 times the bilayer core the interfacial strength decreases, comparable to homogeneously hydrophobic probes. Analytical calculations and molecular dynamics simulations predict a transition between a 'fused' interface and a 'T-junction' that matches the experimental results, showing lipid disorder and defect formation for thicker bands. These results show that matching biological length scales leads to more intimate bio-inorganic junctions, enabling rational design of non-destructive membrane interfaces.

Introduction

Nanomaterials and nanostructured surfaces offer new opportunities to interact with biological species at their native length scales, promising more effective interfaces if the appropriate architectures can be discovered. In particular, engineered interfaces between nanostructures and lipid bilayers, themselves nanoscale two-dimensional fluids approximately 5 nm thick, may provide a unique means to breach this defensive wall enabling direct chemical and electrical access to the cell's interior. Technologies for drug delivery, electrical ion-channel measurements, single cell analysis, and gene therapy would all benefit from an improved understanding of how to establish direct chemical and electrical conduits to the cell's interior without inducing detrimental side effects. While there are existing methods for gaining intracellular access, the techniques tend to be destructive (electroporation and patch-clamping), slow (microinjection and patch-clamping), or inefficient (liposomal delivery and endocytotic uptake).

Recent results have shown that nanowires,[1–3] nanoparticles,[4,5] and nanostructured[6] materials may directly penetrate the lipid bilayer, and in some cases do not overtly affect cell function. However, the actual interface between these penetrating materials and the lipid bilayer is largely unknown, and the extent to which nanoscale features are important is not fully understood. Work by Stellacci and coworkers has shown that molecular scale hydrophobic patterning on nanoparticles presents a mixed-philicity surface able to be accommodated in both hydrophilic and hydrophobic domains, though the adhesion strength is unclear.[4,7] Porous or weak interfaces can lead to fluid and electrical leakage, mechanical instability, and cytotoxicity, thus making the biotic/abiotic junction as well-integrated as possible a crucial goal. Here we demonstrate that the size of nanostructured hydrophobic bands on membrane penetrating probes can control the interaction strength and morphology of the inorganic–lipid interface, providing a rational architecture for reliable and non-destructive through-membrane access.

The lipid bilayer itself is composed of two lipid leaflets, and consists of three different zones: external hydrophilic head groups, hydrophobic lipid tail groups that form the lipid core, and internal hydrophilic head groups. In their liquid state, lipids in the bilayer are highly mobile species, with the structure a dynamic balance between the hydrophobicity of the tail groups, stretching/compression of the tails, head group repulsion, and the relative head to tail dimensions.[8] Because of this mobility, a wide array of lipid bilayer structures has been observed, including vesicles, lamellar sheets, triple junctions, tubules, and platelets.[9] Small molecules and even some nanoparticles[4,5] are able to partition into and through the bilayer without dramatically altering its organization, however, when larger materials penetrate the bilayer an edge or interface must be created. The structure of this new interface is not clear, yet would be anticipated to depend upon the material's nanoscale morphology and hydrophilicity.

Fig. 1 shows four general scenarios for the bilayer interface structure after material penetration. The first is a 'fused' state (Fig. 1a), where the bilayer makes intimate contact with the probe with little or no disruption of the lipid organization. This is most reminiscent of transmembrane protein interfaces, which often have the first layer of lipids transiently adsorbed on the protein surface.[10] The uninterrupted hydrophobic layer and tight interface serve as a significant barrier for ion or fluid flow, preventing exchange from one side of the membrane to the other. Indeed, cell membranes can have electrical resistances ranging from 10–100 GΩ,[11,12] implying almost no ion leakage occurs at the thousands of protein–membrane interfaces. This scenario likely requires nanoscale modification of the probe surface, since it simultaneously interacts with both the hydrophilic and hydrophobic zones of the lipid bilayer.

[a]*Department of Materials Science and Engineering, Stanford University, 476 Lomita Mall, Stanford, California, 94305, USA. E-mail: nmelosh@stanford.edu*
[b]*Department of Mechanical Engineering, Stanford University, 476 Lomita Mall, Stanford, California, 94305, USA*

† Electronic supplementary information (ESI) available: Breakthrough rate as a function of force plots for 5 nm, 10 nm and ∞-probes. See DOI: 10.1039/c0nr00486c

Published on 07 October 2010 on http://pubs.rsc.org | doi:10.1039/C0NR00486C
Downloaded on 17 February 2011

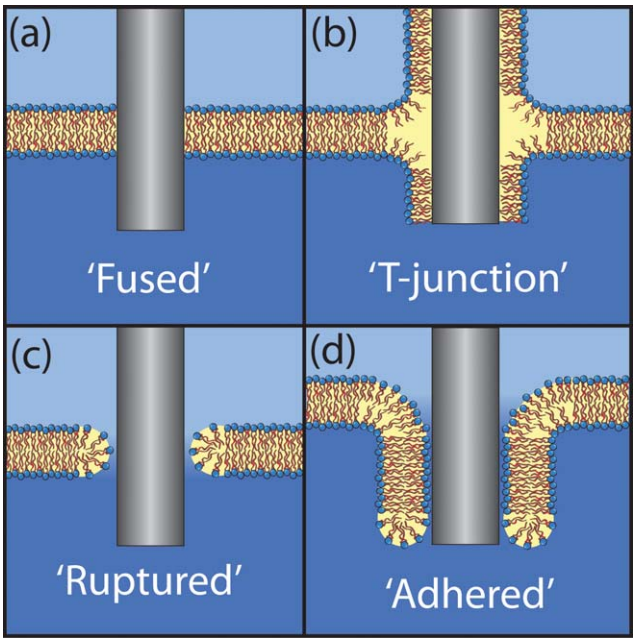

Fig. 1 Different possible scenarios of lipid interfaces to penetrating probe materials.

The second possible structure is the 'T-junction', Fig. 1b. This architecture essentially splits the bilayer into two monolayers in which each contact the probe surface, similar to triple-bilayer junctions observed in the hemifusion state during membrane fusion.[13,14] This arrangement may be energetically favorable for hydrophobic probes, since the surface is in contact with the hydrophobic bilayer tails. A key aspect to this arrangement is the formation of an unfavorable empty interstice, or void, where the bilayer splits, estimated to cost $\sim$10 k_bT per nm length of interstice.[15,16] In hemifused junctions between flexible lipid vesicles this energy can be reduced by increasing the local curvature and lipid splay,[13] however, in this case the bilayer must conform to the stiff probe surface and is thus largely unable to do so. This state may therefore be weaker than the fused state. Related structures, such as membrane stalks, have been predicted to increase the rate of hole formation in the surrounding membrane, which could also destabilize this interface.[17–19]

The third situation is the 'ruptured' state where the bilayer forms a hole around the probe with a hydrophilic lipid edge near the probe surface but not in direct contact (Fig. 1c). This may be the favored configuration for hydrophilic probe surfaces since both materials are in continuous contact with water, however, the gap allows fluid and ions to diffuse through the interface. The leakage rate through the junction could vary greatly depending upon the separation between the edge and the probe surface and may fluctuate over time. Energy considerations and molecular dynamics simulations imply that the ruptured bilayer edge consists of a hemispherical cap of lipids which shield the hydrophobic core from the aqueous phase.[20,21] The curvature and partial exposure of the tail groups make the edge a relatively high energy state, with line energies on the order of 10 pJ m^{-1}.[21–23] This is still considerably smaller than direct lipid tail–water contact, which can be estimated using typical alkane–water surface energies of 25 mJ m^{-2} to be roughly 75 pJ m^{-1} for a 3 nm thick bilayer core.[8] While at equilibrium holes in the membrane are unusual, they are commonly created by artificial means such as electroporation[24] or mechanical tension,[22,25] thus are not unlikely for penetrating probes.

The final scenario is the 'adhered' state (Fig. 1d), in which the lipid surface is attached to the surface of the probe. Lipid–surface adhesion is common in supported lipid bilayers, driven by electrostatic and van der Waals attractions.[26] The lipid is usually not in direct contact with the surface, instead separated by a 1–2 nm aqueous gap.[27,28] This gap allows some ion transport through the junction as measurements have found conductivities of $\sim$0.002 Ω^{-1} cm^{-1} for model lipid/glass interfaces,[29] yet larger proteins may be prevented from passing. This is thought to be the interface created during patch-clamp measurements, and with sufficient surface contact area could be highly resistive.

The specific nature of the probe/lipid junction is important for the mechanical strength, electrical resistivity, and cytotoxicity of the interface. For non-destructive interfaces to cells and membranes, the fused state is likely optimal by preventing leakage from the cytosol and maintaining strong attachment. We recently demonstrated that by mimicking the structure of transmembrane proteins with nanoscale hydrophobic bands around cylindrical atomic force microscope (AFM) tips, the 'stealth' probes spontaneously inserted into lipid membranes and formed strong interfaces.[6] The concept is that by matching the width of the hydrophobic bilayer core with a hydrophobic stripe on an otherwise hydrophilic surface, the lipids would form a seamless interface, even with a sizable diameter probe (Fig. 2). Electrical measurements further confirmed that this interface was tight with respect to ion motion, with average resistances over 3 GΩ.[30] Surprisingly, the interfacial strength was not solely governed by the hydrophobicity of the nanoscale bands, but is also influenced by the identity of the hydrophobic molecules used, with butanethiol and dodecanethiol showing very different behavior.[6]

While this was an important step towards controlling the formation of membrane-penetrating bio-interfaces, the significance of band thickness relative to bilayer thickness was not fully explored. As the band gets thicker relative to the bilayer core the lipids must undergo increasing reorganization, which could weaken the interface. In this study we examine a systematic series of band thicknesses using AFM interfacial strength measurements with butane and dodecane thiols, combined with molecular dynamics (MD) simulations to reveal the local molecular configurations. We find both the adhesion strength and organization have significant dependencies on the thickness of the hydrophobic band, highlighting that matching the native biological nanoscale dimensions is critical for forming intimately connected bio-inorganic interfaces.

Results and discussion

Biomimetic stealth probes with Au bands 2, 5, or 10 nm in width were fabricated from commercial silicon AFM cantilevers using a combination of focused ion beam (FIB) milling and metal deposition, as shown in Fig. 2.[6] The width was defined from the thickness of an evaporated Au film sandwiched between Cr layers, which could be controlled to be within $\pm$5%. Hydrophobic molecules were self-assembled onto the exposed edge of the Au layer after FIB milling to complete the band.

 This journal is © The Royal Society of Chemistry 2011

Published on 07 October 2010 on http://pubs.rsc.org | doi:10.1039/C0NR00486C
Downloaded on 17 February 2011

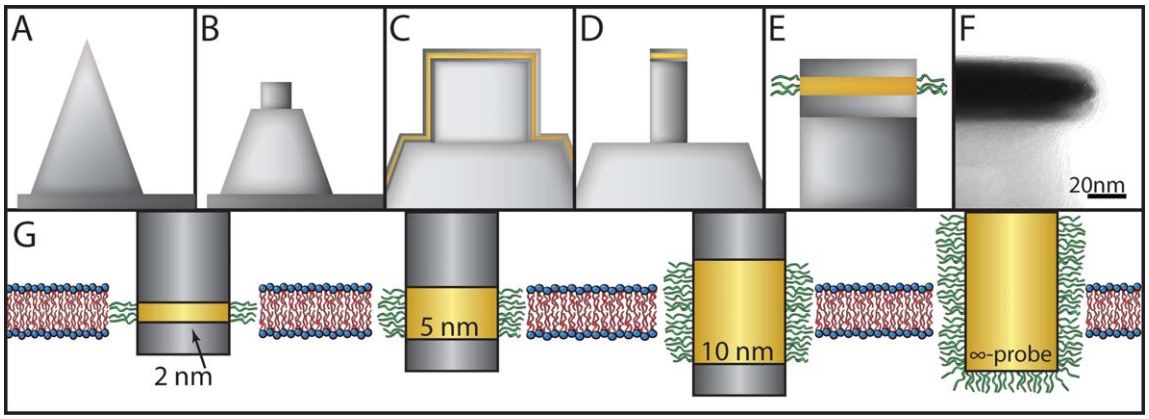

Fig. 2 Fabrication of hydrophobic bands on AFM cantilever probes. (a) Standard Si AFM cantilevers are used as a basis for fabrication. (b) FIB milling is used to create an ~500 nm post. (c) Metal deposition (e-beam, sputtering) is used to deposit a layered Cr–Au–Cr structure. (d) Evaporated tips are re-milled in the FIB to a final diameter of ~200 nm. (e) Au bands are rendered hydrophobic *via* thiol-mediated self-assembly. (f) TEM image of a 10 nm Au band (dark, central band) at the end of a milled post. (g) Probe geometries used in this study.

Homogeneously functionalized posts were also fabricated without the band structure for comparison, hereafter referred to as ∞-probes (Fig. 2). Since we had previously found the molecular structure of the hydrophobic functional molecules impacted the interface strength, both butanethiol and dodecanethiol were examined.

The interfacial strength of the probe/lipid junction was measured by pushing the functionalized AFM probe tips into a stack of 2 : 1 SOPC : cholesterol lipid bilayers using a force-clamp approach (Fig. 3). In this technique, the probes are rapidly loaded to a large force (~60 to 100 nN) against a stack of lipid bilayers by advancing the *z*-piezo. Following loading, the *z*-piezo is fixed in position and the cantilever deflection monitored as a function of time as the probes break through each bilayer, penetrating deeper into the stack and reducing the applied load. The resulting displacement or force curves display characteristic stair–steps consisting of rapid jumps when a bilayer fails, followed by uniform plateaus when the tip is loaded on a fresh bilayer (Fig. 3b). By combining several series of curves, the average breakthrough rate (the inverse of the time to failure) as a function of force can be tabulated (Fig. 3c).

The interface strength is then calculated assuming that the probe tear-out and penetration process can be described as crossing an energy-barrier with a set barrier height and position. Many mechanical systems such as protein binding strength and bilayer rupture[31–33] follow a simple Langevin reaction model under an applied force, which leads to an enhanced reaction rate as a function of load:

$$k = A \exp\left(-\frac{E_0 - F\gamma}{k_b T}\right) \quad (1)$$

where k is the failure rate at a given force, A is the attempt frequency (the cantilever resonance frequency of ~6 kHz was used[34]), E_0 is the unstressed energy barrier height, F is the applied

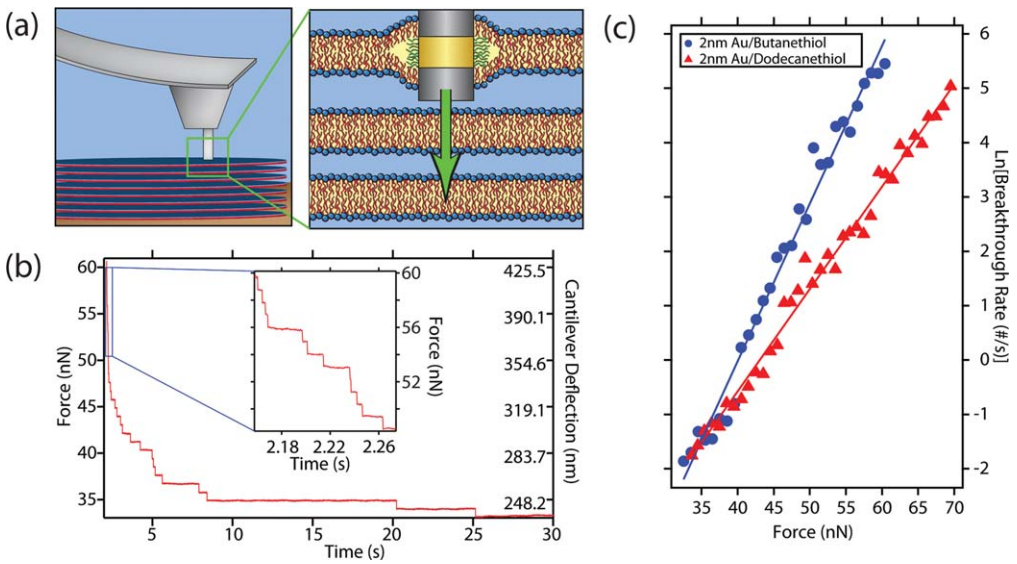

Fig. 3 AFM measurements of lipid–probe interface strength. (a) Stealth probes pressed against a stack of lipid bilayers, causing the tip to jump from bilayer core to bilayer core as it penetrates the stack. (b) Testing results in characteristic stair–step curves as a function of time. (c) The breakthrough rate as a function of force is plotted in order to extract the unstressed energy barriers for each probe (see Fig. S1† for 5 nm, 10 nm and ∞-probe plots).

Published on 07 October 2010 on http://pubs.rsc.org | doi:10.1039/C0NR00486C
Downloaded on 17 February 2011

force, T is the absolute temperature, and γ is the location of the energy barrier. By fitting ln (k) as a linear function of force, both E_0 and γ can be determined (Fig. 3c). The value of the energy barrier reflects both the energy necessary to tear the probe free of the bilayer (the adhesion strength) as well as penetrate the bilayer below it, thus is most properly used to compare strengths between different structures rather than for absolute interfacial energy. This calculation of E_0 should also be taken as a lower bound due to the uncertainty of the actual attempt frequency, A, which is likely significantly higher than the cantilever resonance frequency.

The failure energy measurements clearly show that the interfacial strength decreases with increasing band thickness (Fig. 4). For the butanethiol functionalization, the 2 nm band has a high strength of $E_{0,2nm} = 20.3 \pm 0.4$ k_bT, which is maintained for 5 nm thick bands ($E_{0,5nm} = 21.8 \pm 0.9$ k_bT). However, the strength dramatically decreases for 10 nm thick bands to $E_{0,10nm} = 15.3 \pm 0.8$ k_bT, which is equivalent to the ∞-probes ($E_{0,\infty} = 16.2 \pm 0.7$ k_bT). This emphasizes the importance of matching the inherent nanoscale dimensions, as the 10 nm band, which is just two to three times the thickness of the hydrophobic bilayer core, is functionally equivalent to the infinitely thick case. Dodecanethiol functionalized probes show similar behavior, with 2 nm bands having the highest adhesion energy ($E_{0,2nm} = 16.8 \pm 0.2$ k_bT). However, at 5 nm band thicknesses the interface strength has already started to decrease, reaching a value of $E_{0,5nm} = 14.0 \pm 0.6$ k_bT and decaying further to $E_{0,10nm} = 10.9 \pm 0.6$ k_bT at 10 nm thick. Once again the 10 nm case is equivalent to the ∞-probe ($E_{0,\infty} = 11.1 \pm 0.4$ k_bT).

In agreement with our previous results,[6] butanethiol functionalized probes display larger energy barriers than dodecanethiol for all probe geometries. The energy offset between the two functionalizations is very similar for the 2, 10, and ∞-probe cases (3–5 k_bT). This suggests that each molecular functionality has a different fundamental interface strength with the bilayer, and the trend observed with band thickness is strictly due to geometry. If the lipid interface to the different molecules changed dramatically we would expect the relative strengths to change as well. The fact that dodecanethiol showed a pronounced strength decrease at 5 nm not present for butanethiol indicates the transition from a stable to weak interface occurs at thinner bands for dodecanethiol. We speculate this may be due to the crystallinity of the dodecanethiol monolayers[6] which may be disrupted at very thin band thicknesses, however, this has not been demonstrated at this point.

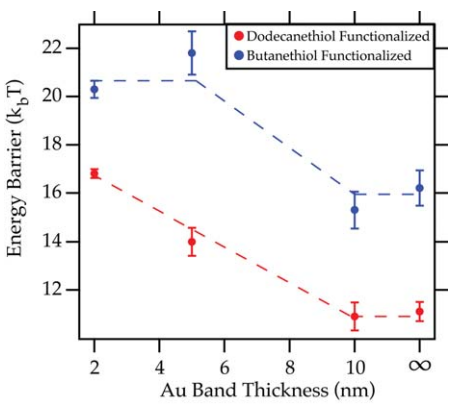

Fig. 4 Interfacial strength for a series of different hydrophobic band thicknesses using butanethiol (blue) or dodecanethiol (red) functionalization. Lines added to guide the eye.

The ability of lipid bilayers to accommodate the different band thicknesses can be compared to the bilayer deformations observed for length-mismatched transmembrane proteins.[35] For example, when linear gramicidins, a natural antibiotic peptide from *Bacillus brevis*, dimerize in opposing bilayer leaflets the resulting hydrophobic transmembrane domain length often varies from that of the host bilayer core.[36] When gramicidin is added to synthetic lipid bilayers, X-ray lamellar diffraction experiments detect an increase in the phosphate-to-phosphate distance from 30.8 Å to 32.1 Å for DLPC bilayers, which have a thinner core than the protein, and a decrease from 35.3 Å to 32.7 Å for DMPC bilayers, which have a thicker core than gramicidin.[37] It has also been shown that a reduction in the bilayer compression and bending moduli can mitigate the decrease in channel lifetimes associated with increasing hydrophobic mismatch.[38] These studies all suggest the bilayer is able to deform to match the hydrophobic protein domain size as opposed to channel distortion or rotation.

The feasibility of the bilayer deforming to create a fused interface for the 2 nm and 5 nm band thicknesses was estimated from the deformation energy based on the theory developed for transmembrane protein-induced distortions. Bilayer deformation energy due to hydrophobic mismatch, ΔG_{def}, was calculated from the bilayer spring constant, H_B, the degree of mismatch between the length of the probe's hydrophobic band, l_p, and the length of the hydrophobic bilayer core, l_b:[39]

$$\Delta G_{def} = H_B(l_p - l_b)^2 \quad (2)$$

assuming the intrinsic curvature of an isolated lipid monolayer is negligible.[40] H_B is a function of bilayer area-compression modulus, K_a, the bending modulus, K_c, l_b, and the radius of the bilayer inclusion (in this case, the radius of the stealth probe). Using the scaling relations derived by Nielsen and Andersen[39] and assuming $K_a = 290$ pN nm^{-1} and $l_b = 3.1$ nm for 2 : 1 SOPC : cholesterol bilayers,[6,40] H_B is found to be 2280 k_bT nm^{-2} for a 200 nm diameter probe. The deformation energy for each band thickness is listed in Table 1. These are compared with the energy necessary to expose the hydrophobic region (ΔG_{phobic}) of either the bilayer core (for $l_p < l_b$) or the functional band (for $l_p > l_b$). With an alkane–water surface energy[8] of ~25 mJ m^{-2} and a probe radius of 100 nm, it becomes energetically beneficial to deform the bilayer to match band thicknesses of approximately $1.4 < l_p < 4.8$ nm (Table 1).

These calculations suggest the fused interface geometry is favorable for 2 nm stealth probes with a slight bilayer compression, similar to transmembrane proteins. The 5 nm band

Table 1 Calculated bilayer distortion energies (ΔG_{def}) and hydrophobic exposure energies (ΔG_{phobic}) per nm of interface perimeter for each band thickness. Lowest calculated energies are italicized

l_p/nm	l_b (%)	ΔG_{def} per nm/k_bT nm^{-1}	ΔG_{phobic} per nm/k_bT nm^{-1}
2	64.5	*4.3*	6.7
5	161.3	13.1	*11.6*
10	322.6	173.0	*42.0*

This journal is © The Royal Society of Chemistry 2011

Published on 07 October 2010 on http://pubs.rsc.org | doi:10.1039/C0NR00486C
Downloaded on 17 February 2011

is just outside the calculated stability range (1.5 k_bT higher energy), which would make the interface sensitive to other factors such as molecular structure. Both of these predictions are consistent with adhesion strength experiments. The 2 nm bands had the highest interfacial strength for either functionalization, and while the 5 nm butanethiol probes maintained their strength, dodecanethiol weakened slightly. For 10 nm probes the deformation energy is more than 130 k_bT higher than the hydrophobic surface energy, thus fused interfaces are prohibitory. This is supported by the equivalent behavior of the 10 nm and ∞-probes, showing a fused interface is not formed.

However, these calculations only apply to the fused interface and do not account for the other possible geometries shown in Fig. 1, which may have lower interfacial energies. While the energy of a 'T-junction' is currently unknown, a rough estimate may be provided by considering the junction to consist of an interstitial void and two rounded hydrophilic one-half caps that form at the band/hydrophilic probe edges. This assumes negligible energy penalty at the alkane/lipid monolayer interface. The void energy is ~10 $k_bT\ nm^{-1}$,[15] while the cap energy is derived from the hydrophilic edge energy, about 2.5 $k_bT\ nm^{-1}$.[22] The sum of these components puts the 'T-junction' energy around ~13 $k_bT\ nm^{-1}$, which is surprisingly close to the calculated deformation energy values at the experimental transition thickness. Moreover, the energy for a T-junction to a 10 nm band would be equivalent to a 20 nm band or an ∞-probe, since the larger monolayer/alkane interface does not add additional energy, consistent with observations.

The 'ruptured' and 'adhered' junctions are also less likely due to the interface strength's dependence on molecular functionalization for the ∞-probes. The ruptured state has no direct contact with probe, thus the energy barrier for each ∞-probe functionalization should converge to a common value. Instead, there is a consistent ~5 k_bT offset. The adhered state is highly energetically unfavorable due to the hydrophilic lipid/hydrophobic probe contact. This could be avoided if another species (such as excess lipid) coated the probe first to make it hydrophilic, yet again there should be no dependence on molecular functionalization in this event. From this set of observations, we conclude that the T-junction is the most likely structure for bands thicker than 5 nm.

Molecular dynamics simulations

The molecular structure of the interface between the nanoscale hydrophobic band and lipid bilayer was further examined through a series of molecular dynamics simulations of planar lipid bilayers coming into contact with hydrophobic bands of different thicknesses. Since this interaction is expected to involve significant rearrangements of lipid bilayer around the hydrophobic band, we chose a coarse-grained lipid model to allow membrane undulations and peristaltic motions (thickness fluctuations). Large scale lipid reorganization such as self-assembly of micelles is known to occur on timescales on the order of 10 ns, while 100 ns are needed to capture the shape fluctuations, necessitating a coarse-grained approach to achieve sufficient integration times.[41,42] Coarse grained or unified atom models represent small groups of atoms by single interacting 'beads',[41,43–45] and have been used extensively to study amphiphilic molecular phase behavior, agglomeration, self-assembly, and large scale shape fluctuations.[41,43,46,47]

A lipid model was constructed according to Goetz and Lipowsky, comprised of strings of particles which interact *via* a Lennard-Jones type interaction potential that is purely repulsive for water–oil interactions but contains short range attraction for like particles.[41] This model was previously used to semi-quantitatively describe both molecular scale phenomena such as lipid aggregation or diffusivity in bilayers, and continuum scale phenomena such as membrane elasticity, interfacial tension and membrane bending.[41,43] In our model, the system is built up from three types of particles (Fig. 5): hydrophilic solvent particles, representing water particles and denoted by '*w*'; hydrophilic lipid head group particles denoted by '*h*'; and hydrophobic particles for both the alkanes and the tails of the lipids denoted by '*t*'.[41] The lipids are modeled as a linear chain of one hydrophilic head group particle and five hydrophobic particles for the tail, and the hydrophobic alkane molecules in the band are treated as a linear chain of four hydrophobic particles.

Hydrophobic bands representing the stealth probes were constructed from rows of alkanes tethered on one face of a simulation cell in a straight line. We assume that the curvature of the experimental probe (200 nm diameter) is small relative to the lipid dimensions, and thus approximated as a flat surface. Adjacent alkanes were tethered at a spacing of 4 Å which is close to the alkanethiol packing observed on the gold surface.[48] To mimic the hydrophilicity of the chromium oxide coated AFM probe, solvent particles were fixed at regular intervals on the remaining area of simulation box face. The hydrophobic ∞-probe was represented by tethering alkanes on the entire face.

The starting configuration of the system was a continuous, fully relaxed bilayer oriented parallel to an alkane band anchored at one side of a periodic-boundary condition simulation box (Fig. 6a). While this orientation is different than the experimental stack-penetration, it avoids artifacts caused by presupposing a particular edge structure, which would be necessary for any other bilayer configuration. It is also more representative of the case of individual flexible lipid bilayers, such as cell membranes. This arrangement does tend to predispose the overall geometry to adopt a tri-bilayer junction, however, it allows the bilayer to reorganize and expand its area with relative ease, such that the interfacial structure close to the band is still the lowest energy state. The 'fused' and 'T-junction' states (Fig. 1) are thus most

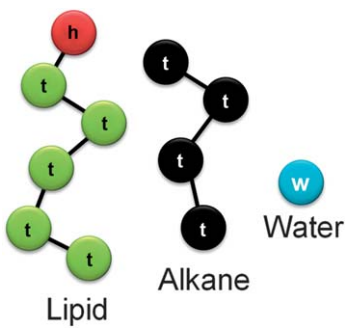

Fig. 5 Models for various molecules used in the simulation, made up of three kinds of particles: *h*—hydrophilic head, *t*—hydrophobic tail, *w*—water.

Published on 07 October 2010 on http://pubs.rsc.org | doi:10.1039/C0NR00486C
Downloaded on 17 February 2011

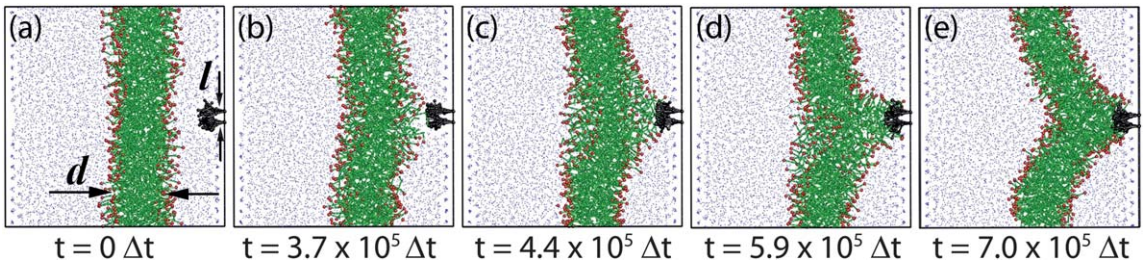

Fig. 6 Time-resolved fusion of lipid bilayer with hydrophobic band for band thickness, $l = (2/5)d$. Configurations at various intermediate time points during the simulation are depicted. It took 7×10^5 time steps for the fusion to complete. Each frame is a projection of a three dimensional simulation box with periodic boundary conditions.

properly differentiated by the presence of a void region in the middle of the junction, rather than overall symmetry.

Fig. 6 shows the time-resolved reorganization of the bilayer for a band thickness, $l = (2/5)d$, where d is the equilibrium thickness of the bilayer (see Methods section for details). The initial distance between the bilayer mid-plane and the wall face with tethered alkanes was set at 1.5 times the bilayer thickness as shown in Fig. 6a. This separation is chosen such that the range of non-bonded interactions between the alkanes and lipids barely overlap. For the first 3.0×10^5 time steps, the bilayer shows no visible effect of alkane interaction, and undulates. After $\sim 3.0 \times 10^5$ time steps, frequent lipid protrusions from the bilayer leaflet close to the band are observed. At 3.5×10^5 time steps, coordinated rearrangement of lipids begins as several lipid tails come in contact with the band (Fig. 6c). A well defined contact region begins to take shape around 4.0×10^5 time steps as many more lipid tails align with the alkane molecules. The interface at this point is established only at one small region along the length of the band. Subsequently, the fused interface extends along the length of the band, rapidly integrating the entire band with the hydrophobic core of the bilayer. By 6.0×10^5 time steps, the bilayer leaflet in the vicinity of the band is fused completely; however, the opposite leaflet is still disordered. It takes about 7.0×10^5 time steps for this leaflet to order and the interface to reach its final structure. This is an ordered 'fused' state, as indicated by the absence of any void regions or hydrophilic head groups trapped in the hydrophobic core, and the band is completely fused with the hydrophobic bilayer core. This structure was stable until the end of the experiment at 1.0×10^6 time steps.

To study the effect of hydrophobic mismatch in this system and compare to experimental results, the thickness of the hydrophobic band was varied by tethering additional rows of alkanes on the face of the simulation box. Fig. 7 shows the interface structure between the bilayer and hydrophobic band for different band thickness, while Fig. 8 shows different projections and the 3D simulation box for $l = (2/5)d$ and $l = (8/5)d$. For band thicknesses $l = (2/5)d$, $(3/5)d$, and $l = d$, a uniform 'fused' interface is observed in all cases with a well defined hydrophobic core and no interstitial voids. In the top view of Fig. 8a, the interface is clearly homogenous over the entire length of the hydrophobic band. Interestingly, the time to form the interface increases from 6.5×10^5 time steps for $l = (2/5)d$ to 1.0×10^6 time steps for $l = (3/5)d$ to 1.5×10^6 time steps for $l = d$. Since the number of lipids that participate in the interface and the extent of bilayer rearrangement required scales with the band thickness, this trend is

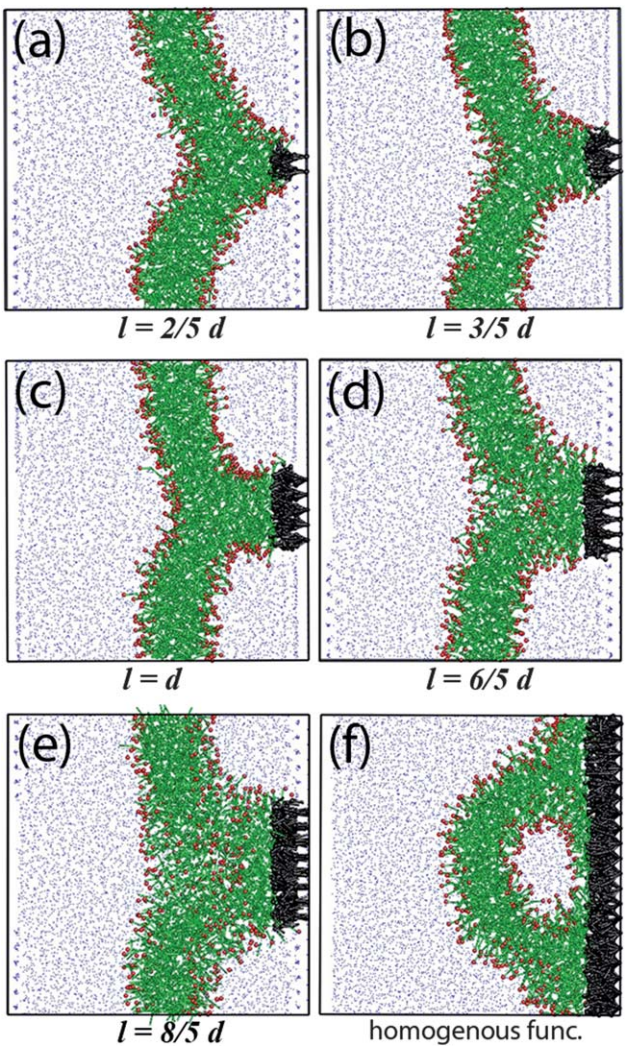

Fig. 7 Equilibrium interface structures formed after ~ 1 to 1.5×10^6 time steps for various hydrophobic band thicknesses, where l is band thickness, and d is bilayer thickness. (a) $l = (2/5)d$—bilayer fused with band, homogenous and ordered interface. (b) $l = (3/5)d$—bilayer forms 'fused' interface with band. (c) $l = d$—bilayer fused with band, no void formation. (d) $l = (6/5)d$—bilayer fuses to the band, small interstice void formed. (e) $l = (8/5)d$—disordered fusion, large interstice void formed with a bilayer pore (see also Fig. 8). (f) Homogenous functionalization resembling ∞-probes. Bilayer fuses to surface in a 'T junction' by splitting into two monolayers. Small interstices present, yet pores common.

This journal is © The Royal Society of Chemistry 2011

Published on 07 October 2010 on http://pubs.rsc.org | doi:10.1039/C0NR00486C
Downloaded on 17 February 2011

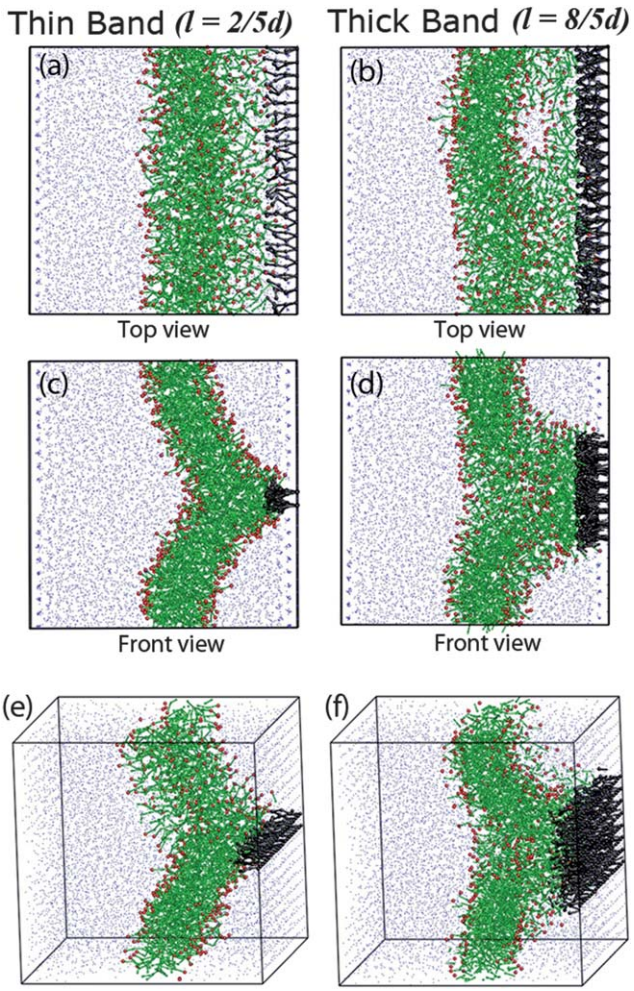

Fig. 8 Different views of equilibrium interface structures formed after ~1 to 1.5 × 10^6 time steps for $l = (2/5)d$ and $l = (8/5)d$. (a) Top view for $l = (2/5)d$ shows uniformity of interface along band length. (b) Top view for $l = (8/5)d$ shows a bilayer pore indicating leaky and weak interface. (c) Front view for $l = (2/5)d$ bilayer fused with band, homogenous and ordered interface. (d) Front view for $l = (8/5)d$ incomplete fusion, heterogeneous disordered interface. (e) 3-D view of equilibrium interface structure for $l = (2/5)d$. (f) 3-D view of equilibrium interface structure for $l = (8/5)d$.

not surprising. Moreover, the structure gradually transitions from being relaxed with a uniform curvature for $l = (2/5)d$ to a tri-bilayer structure for $l = d$, though at the alkane interface all are 'fused' into the bilayer.

Hydrophobic bands with thicknesses of $(6/5)d$, $(8/5)d$, or infinite produced ill-defined structures with disordered interfaces. As the hydrophobic core of the bilayer comes in contact with the hydrophobic band, voids start appearing at the junction. These voids cause the lipids in the vicinity to flip (indicated by the red head groups in the tail region, Fig. 7d and e), disrupting the ordered structure of the bilayer. The structure also varies along the length of the band indicating the formation of a weak interface. At $l = (8/5)d$, membrane pores form at the interfacial region, as shown in the top view in Fig. 8b. In addition to allowing fluid leakage, pores are known to be nucleation sites for rupture fronts in lipid bilayers, further weakening this structure.[49,50] These two cases show evidence for a disordered T-junction state in equilibrium with membrane holes. Fig. 7f shows the bilayer structure with a homogenously functionalized ∞-probe after 1.5 × 10^6 time steps. The bilayer has split to form two clearly defined T-junctions, with hybrid lipid monolayer/alkane interfaces along the probe length. The remaining lipid not in contact with the surface reorganized into a tubular geometry. This particular structure may be a result of the fixed number of lipids in the system, as fewer free lipids are available after the formation of the lipid monolayer, favoring lipid tubules which often form at lower lipid concentrations.[41]

The structures formed as the hydrophobic band thickness increases strongly corroborate experimental findings and provide a qualitative understanding of the experimental trends. Assuming the bilayer thickness in the experiments to be about ~5 nm (including head groups), bands with thicknesses $l = (2/5)d$ and $l = d$, resemble the 2 nm and 5 nm bands, respectively. From the simulation results, these thin bands spontaneously form well-ordered, 'fused' interfaces that are uniform along the entire band length (Fig. 7a–c). Since this interface lacks defects or other high energy regions like high curvature areas, it is expected to have a high barrier to failure, in line with experimental findings. It should be noted that while both butanethiol and dodecanethiol were used in experiments, the simulations were performed for a generic alkane molecule. Lack of a 3-body term in the alkane model ensures that the alkanes never crystallize, thus the model is more representative of shorter molecules like butanethiol.

Similar to experiments, there is a distinct transition as the band thickness becomes larger than the bilayer thickness. The $l = (6/5)d$ and $l = (8/5)d$ simulations, roughly equivalent to ~6 and 8 nm bands, showed dramatically worse organization, as might be expected for the 10 nm thick band result. For such thick band probes, the interface structure appears to be a disordered T-junction with interstitial voids that is heterogeneous along the band length. The T-junction may thus be much less ideal than shown in Fig. 1b, and in fact exist in combination with the fused junction. The co-existence of these two phases is also supported by the partial weakening of the 5 nm dodecanethiol probes, without complete decay to the 10 nm case. For homogenous functionalization that mimics ∞-probes (Fig. 7f), the T-junction structure is much clearer, yet still has defects in the form of voids that cause lipids in the vicinity to disorder. The presence of defects and heterogeneities in the interface structure for these cases could likely result in low interface strengths, in agreement with experimental observations.

Conclusion

Seamlessly integrating inorganic probes into cell membranes is an exciting goal for establishing long-term, non-destructive bio-interfaces. Here we show that biomimetic probes with nanoscale hydrophobic bands can fuse into the hydrophobic lipid bilayer core. The interfacial strength was highly sensitive to band thickness, with the strongest interfaces formed for 2 nm thick bands. Both the analytical calculations and MD simulations predicted that as the band thickness exceeded 5 nm the 'fused' interface would no longer be stable, which was also observed experimentally. The agreement between these three different approaches is surprisingly good, indicating that the models

Published on 07 October 2010 on http://pubs.rsc.org | doi:10.1039/C0NR00486C
Downloaded on 17 February 2011

developed for transmembrane proteins may also be applied to inorganic devices. The structure of the lipid–probe interface for bands above 5 nm thick is most likely a T-junction state based on analytical energy estimates, MD simulations, and the adhesion strength's dependence on molecular functionality for both the 10 nm and ∞-probes. These junctions have low interfacial strengths, and simulations show disordered interfaces and a propensity for hole formation. This unstable interface may also help explain why homogenous hydrophobic coatings on patch-clamp electrodes do not enhance the electrical seal resistance.[51] On the other hand, thin hydrophobic bands have strong adhesion strengths and well-ordered molecular interfaces, consistent with recent electrical measurements which found very high seal resistances for these probes.[30] Further atomistic MD simulations would be useful to examine the detailed molecular structure near these bands, and to understand the role of different molecular functionalizations. The fact that nm thick bands successfully integrated into lipid membranes shows that matching the nanoscale dimension of biological materials can provide significant benefits for bio-inorganic interfaces, and create an array of new opportunities for drug delivery, electrical measurements and single cell analysis.

Materials and methods

Stealth probe fabrication

Standard commercial AFM cantilevers with a nominal spring constant of 0.08 N m^{-1} (CSC-38/Al BS, MikroMasch USA) were mounted vertically in an FIB (FEI Strata 235 DB). The tips were milled to a post shape 500 nm in diameter and 600 nm long using a 30 kV, 10 pA Ga-beam. The tips were then rotated 90° onto their sides and milling repeated to complete the post-geometry (Fig. 2b). A layered Cr–Au–Cr structure (each Cr metal layer = 5 nm thick and Au layer = 5 or 10 nm) was deposited by e-beam metal evaporation (Temescal) on the modified AFM cantilevers at a rate of 0.5 nm s^{-1} (Fig. 2c) for the 5 nm and 10 nm Au band tips. For 2 nm probes, to deposit the layered Cr–Au–Cr structure (bottom Cr layer = 5 nm and Au layer = 2 nm; top Cr layer = 3 nm), dc magnetron sputtering with 20 mTorr Ar gas in an ultrahigh vacuum chamber of base pressure ~6.2 × 10^{-9} Torr was utilized. Cr was deposited at a rate of 0.575 Å s^{-1}, while Au was deposited at a rate of 0.177 Å s^{-1}. ∞-Probes were fabricated in a similar manner, except 10 nm Cr was deposited, followed by 20 nm of Au. Thicknesses are ±5% and were calibrated using X-ray reflectivity. Following metal deposition, the cantilevers were re-milled in the FIB to a final diameter of approximately 200 nm using the same milling procedure, with the exception of the beam current being reduced to 1 pA (Fig. 2d).

Formation of lipid bilayer stacks

Stacks of 30–2000 lipid bilayers were formed by gentle hydration of a dried lipid cake. Glass coverslips (VWR, 25 mm dia.) were cleaned for 30 min in Piranha etch. Coverslips were rinsed thoroughly with deionized water and dried under nitrogen. Ten microlitre drops of 10 mg mL^{-1} of a 2 : 1 1-stearoyl-2-oleoyl-*sn*-*glycero*-3-phosphocholine (SOPC) and cholesterol (Avanti Polar Lipids) solution in chloroform were deposited on the clean coverslips, dried under a stream of nitrogen and desiccated under vacuum overnight. Desiccated coverslips were mounted in an Asylum Research closed fluid cell. A strip of PTFE was used to manually spread the dried lipid around the coverslip, forming a thin layer. Following spreading, 1 mL of 1.6% NaCl solution was added to the fluid cell and allowed to hydrate for approximately 2 hours.

Force clamp testing

Membrane probes were functionalized for at least 12 h in 5 mM ethanolic solutions of either 1-butanethiol (Alfa Aesar) or 1-dodecanethiol (Sigma-Aldrich). Previously used tips could be re-functionalized with different molecules following a 30 min UV-ozone cleaning (UVO Cleaner, Jetlight Company Inc.). After UV-ozone treatment, tips were soaked in pure ethanol (Sigma-Aldrich) for 30 min to remove any gold oxide.

Functionalized stealth probes were mounted in an Asylum Research MFP-3D AFM. Spring constant calibration was done using the Sader and thermal methods. Stack penetration curves were obtained by initially bringing the probes into contact with a lipid stack at a rate of 4 μm s^{-1}. Loading was stopped when a force set point of 60–100 nN was reached. Once the set point was obtained, a 30–60 s dwell was triggered where the *z*-piezo position was held constant. During this dwell session, the change in cantilever deflection was measured. Drift in the system was accounted for by leveling the low force/long time drift of the baseline.

Force clamp curves were analyzed by measuring the failure rate and force for each bilayer failure. The failure rate was calculated as the inverse of the failure time, measured from the first point after a breakthrough event to the first point of the following breakthrough. The failure force was the average force during this interval (Fig. 3). The individual failure events were binned in force, and breakthrough rate plotted as a function of force. Energy barriers were then determined by fitting to eqn (1).

Molecular dynamics

Non-bonded interactions between one hydrophilic and one hydrophobic particle were treated with a truncated repulsive soft core potential of the following form:

$$U_9(r) = 4\varepsilon_0\left(\frac{r}{\sigma_{SC}}\right)^{-9} - 4\varepsilon_0\left(\frac{r_c}{\sigma_{SC}}\right)^{-9} + \frac{36\varepsilon_0}{r_c}\left(\frac{r_c}{\sigma_{SC}}\right)^{-9}(r - r_c)$$

Other non-bonded interactions were calculated with a truncated Lennard-Jones potential:

$$U_{6-12}(r) = 4\varepsilon_0\left(\left(\frac{r}{\sigma}\right)^{-12} - \left(\frac{r}{\sigma}\right)^{-6}\right) + Br + A$$

$$B = \frac{4\varepsilon_0}{r_c}\left(12\left(\frac{r_c}{\sigma}\right)^{-12} - 6\left(\frac{r_c}{\sigma}\right)^{-6}\right),$$

$$A = -4\varepsilon_0\left(\left(\frac{r_c}{\sigma}\right)^{-12} - \left(\frac{r_c}{\sigma}\right)^{-6}\right) - Br_c$$

These potentials are truncated such that $U_{9\text{ or }6-12} = 0$ and d $U_{9\text{ or }6-12}/dr = 0$ at $r = r_c$. A uniform cut-off radius of $r_c = 2.5\sigma$ is assumed for all non-bonded interactions. The parameter σ_{SC} is

 This journal is © The Royal Society of Chemistry 2011

chosen to be $\sigma_{SC} = 1.05\sigma$, similar to previous work.[41] For the bonded potential, a harmonic spring force with equilibrium distance σ and spring constant $k = 5000\varepsilon/\sigma^2$ is chosen so that up to 10% of the bonds of a given configuration differ by more than 2% from the long time average bond length equal to σ.[41] The bonded potential is given by:

$$U_{bond}(r) = k(r - \sigma)^2$$

The fundamental scales of length (σ), mass (m) and energy (ε) are chosen such that $N_{AV}m = 36$ g mol^{-1}, $\sigma = 0.33$ nm, and $N_{AV}\varepsilon = 2$ kJ mol^{-1}, where $N_{AV} = 6.022 \times 10^{23}$ mol^{-1}. This implies that each hydrophobic tail particle 't' corresponds to about 2–3 CH_2 groups. Thus, the lipid with 5 tails corresponds to about 13 CH_2 groups, while a four particle long alkane chain is roughly equivalent to dodecane. The temperature is kept constant during the simulation at 324 K which is equivalent to an energy scale of $N_{AV}\varepsilon = 2$ kJ mol^{-1}. The time scale for the model can be calculated from σ, m and ε as $\tau^2 = m\sigma^2/\varepsilon$. For the parameters chosen here, this time scale, τ is ~ 1.4 ps. The time step for the simulation was chosen as 1 fs which is close to $\tau/2000$ used previously.[41]

Molecular dynamics simulations were performed under the NVT ensemble. The size of the box was chosen to be 80 Å × 80 Å × 80 Å. The choice of the number of lipids in the system was based on the previous study of the effect of lipid concentration on membrane tension in a fixed volume system.[41,43] It has been shown that a non-dimensional average head group area of ~2.4 for freely jointed chain lipids similar to the ones used in this study produces bilayers with negligible tension. Any higher or lower lipid densities cause either positive or negative membrane tension, while still assembling into stable bilayers. Using the length scale of $\sigma = 3.33$ Å, for a total projected area of 80 Å × 80 Å, an average head group area of ~2.4 corresponds to about 500 lipids. To keep the volume density of the particles in the box same as previous work, the total number of particles was kept constant at ~9500.[41]

Lipid bilayers, stable for 2×10^6 time steps, are preassembled using a combination of conjugate gradient energy relaxation and molecular dynamics simulation starting from an initially random configuration of molecules. On these timescales, membrane undulations and lipid protrusions can be observed. The equilibrated bilayer is observed to have an average non-dimensional thickness, d of 6, measured as the average separation between parallel planes running through the lipid head groups in each leaflet.

All simulations were performed using the MD++ software package at constant temperature, volume and number of particles.[52] To keep the temperature constant, a Nose–Hoover thermostat was applied.[53,54] The atomic equations of motion were integrated using the Velocity-Verlet algorithm. The time step was fixed at $\Delta t = 1$ fs. With this time step, the fluctuation of the Hamiltonian over 1×10^6 time steps is on the order of 10^2 eV. Since the total energy of the system is on the order of 10^9 eV, this fluctuation is about 7 orders of magnitude smaller, indicating that the choice of time step is adequate. Periodic boundary conditions were applied in all three directions to eliminate any edge effects. Visualization was performed using Atomeye.[52,55]

Published on 07 October 2010 on http://pubs.rsc.org | doi:10.1039/C0NR00486C
Downloaded on 17 February 2011

Acknowledgements

We thank the NSF Center for Probing the Nanoscale grant No. PHY-0425897 and Canon Inc. for support, and B.D.A. acknowledges the NSF CPN for fellowship support. We also acknowledge Evan Pickett for TEM assistance, Steven Kelly and Noureddine Tayebi for help with sputter deposition, and Haneesh Kesari for initial help with simulations.

References

1 W. Kim, J. K. Ng, M. E. Kunitake, B. R. Conklin and P. D. Yang, *J. Am. Chem. Soc.*, 2007, **129**, 7228.
2 A. K. Shalek, J. T. Robinson, E. S. Karp, J. S. Lee, D.-R. Ahn, M.-H. Yoon, A. Sutton, M. Jorgolli, R. S. Gertner, T. S. Gujral, G. MacBeath, E. G. Yang and H. Park, *Proc. Natl. Acad. Sci. U. S. A.*, 2010, **107**, 1870–1875.
3 W. Hällström, T. Mårtensson, C. Prinz, P. Gustavsson, L. Montelius, L. Samuelson and M. Kanje, *Nano Lett.*, 2007, **7**, 2960–2965.
4 A. Verma, O. Uzun, Y. Hu, Y. Hu, H.-S. Han, N. Watson, S. Chen, D. J. Irvine and F. Stellacci, *Nat. Mater.*, 2008, **7**, 588–595.
5 J. Wong-Ekkabut, S. Baoukina, W. Triampo, I. M. Tang, D. P. Tieleman and L. Monticelli, *Nat. Nanotechnol.*, 2008, **3**, 363–368.
6 B. D. Almquist and N. A. Melosh, *Proc. Natl. Acad. Sci. U. S. A.*, 2010, **107**, 5815–5820.
7 J. J. Kuna, K. Voitchovsky, C. Singh, H. Jiang, S. Mwenifumbo, P. K. Ghorai, M. M. Stevens, S. C. Glotzer and F. Stellacci, *Nat. Mater.*, 2009, **8**, 837–842.
8 J. Israelachvili, *Intermolecular and Surface Forces*, Academic Press, San Diego, 1992.
9 *The Structure of Biological Membranes*, ed. P. Yeagle, CRC Press, Boca Ratan, 2nd edn, 2005.
10 A. G. Lee, *Biochim. Biophys. Acta, Biomembr.*, 2003, **1612**, 1–40.
11 B. G. Kornreich, *J. Vet. Cardiol.*, 2007, **9**, 25–37.
12 B. Sakmann and E. Neher, *Annu. Rev. Physiol.*, 1984, **46**, 455–472.
13 Y. Kozlovsky, L. V. Chernomordik and M. M. Kozlov, *Biophys. J.*, 2002, **83**, 2634–2651.
14 L. V. Chernomordik and M. M. Kozlov, *Cell*, 2005, **123**, 375–382.
15 D. P. Siegel, *Biophys. J.*, 1993, **65**, 2124–2140.
16 D. P. Siegel, *Biophys. J.*, 1999, **76**, 291–313.
17 K. Katsov, M. Müller and M. Schick, *Biophys. J.*, 2004, **87**, 3277–3290.
18 M. Müller, K. Katsov and M. Schick, *J. Chem. Phys.*, 2002, **116**, 2342–2345.
19 H. Noguchi and M. Takasu, *J. Chem. Phys.*, 2001, **115**, 9547–9551.
20 J. D. Litster, *Phys. Lett. A*, 1975, **53**, 193–194.
21 F. Y. Jiang, Y. Bouret and J. T. Kindt, *Biophys. J.*, 2004, **87**, 182–192.
22 E. Karatekin, O. Sandre, H. Guitouni, N. Borghi, P. H. Puech and F. Brochard-Wyart, *Biophys. J.*, 2003, **84**, 1734–1749.
23 D. V. Zhelev and D. Needham, *Biochim. Biophys. Acta, Biomembr.*, 1993, **1147**, 89–104.
24 J. C. Weaver and Y. A. Chizmadzhev, *Bioelectrochem. Bioenerg.*, 1996, **41**, 135–160.
25 O. Sandre, L. Moreaux and F. Brochard-Wyart, *Proc. Natl. Acad. Sci. U. S. A.*, 1999, **96**, 10591–10596.
26 T. Cha, A. Guo and X. Y. Zhu, *Biophys. J.*, 2006, **90**, 1270–1274.
27 E. T. Castellana and P. S. Cremer, *Surf. Sci. Rep.*, 2006, **61**, 429–444.
28 B. W. Koenig, S. Kruger, W. J. Orts, C. F. Majkrzak, N. F. Berk, J. V. Silverton and K. Gawrisch, *Langmuir*, 1996, **12**, 1343–1350.
29 R. J. White, B. Zhang, S. Daniel, J. M. Tang, E. N. Ervin, P. S. Cremer and H. S. White, *Langmuir*, 2006, **22**, 10777–10783.
30 P. Verma and N. A. Melosh, *Appl. Phys. Lett.*, 2010, **97**, 033704.
31 E. Evans and F. Ludwig, *J. Phys.: Condens. Matter*, 2000, **12**, A315–A320.
32 E. Evans and K. Ritchie, *Biophys. J.*, 1997, **72**, 1541–1555.
33 S. Loi, G. Sun, V. Franz and H.-J. Butt, *Phys. Rev. E: Stat., Nonlinear, Soft Matter Phys.*, 2002, **66**, 031602.
34 S. Loi, G. Sun, V. Franz and H.-J. Butt, *Phys. Rev. E: Stat., Nonlinear, Soft Matter Phys.*, 2002, **66**, 7.
35 M. Ø. Jensen and O. G. Mouritsen, *Biochim. Biophys. Acta, Biomembr.*, 2004, **1666**, 205–226.

36 O. S. Andersen and R. E. Koeppe, 2nd, *Physiol. Rev.*, 1992, **72**, 89S–158S.
37 T. A. Harroun, W. T. Heller, T. M. Weiss, L. Yang and H. W. Huang, *Biophys. J.*, 1999, **76**, 937–945.
38 T.-C. Hwang, R. E. Koeppe, II and O. S. Andersen, *Biochemistry*, 2003, **42**, 13646–13658.
39 C. Nielsen and O. S. Andersen, *Biophys. J.*, 2000, **79**, 2583–2604.
40 J. A. Lundbæk, O. S. Andersen, T. Werge and C. Nielsen, *Biophys. J.*, 2003, **84**, 2080–2089.
41 R. Goetz and R. Lipowsky, *J. Chem. Phys.*, 1998, **108**, 7397–7409.
42 E. Lindahl and O. Edholm, *Biophys. J.*, 2000, **79**, 426–433.
43 R. Goetz, G. Gompper and R. Lipowsky, *Phys. Rev. Lett.*, 1999, **82**, 221–224.
44 J. C. Shelley, M. Y. Shelley, R. C. Reeder, S. Bandyopadhyay and M. L. Klein, *J. Phys. Chem. B*, 2001, **105**, 4464–4470.
45 S. J. Marrink, A. H. de Vries and A. E. Mark, *J. Phys. Chem. B*, 2004, **108**, 750–760.
46 B. J. Palmer and J. Liu, *Langmuir*, 1996, **12**, 746–753.
47 B. Smit, K. Esselink, P. A. J. Hilbers, N. M. van Os, L. A. M. Rupert and I. Szleifer, *Langmuir*, 1993, **9**, 9–11.
48 A. Ulman, J. E. Eilers and N. Tillman, *Langmuir*, 1989, **5**, 1147–1152.
49 B. V. Deryagin and Y. V. Gutop, *Kolloidn. Zh.*, 1965, **24**, 370–374.
50 K. Olbrich, W. Rawicz, D. Needham and E. Evans, *Biophys. J.*, 2000, **79**, 321–327.
51 B. Sakmann and E. Neher, *Single-Channel Recording*, Springer-Verlag, New York, 1995.
52 V. Bulatov and W. Cai, *Computer Simulations of Dislocations*, Oxford University Press, 2006.
53 S. Nosé, *Mol. Phys.*, 1984, **52**, 255–268.
54 W. G. Hoover, *Phys. Rev. A: At., Mol., Opt. Phys.*, 1985, **31**, 1695–1697.
55 J. Li, *Modell. Simul. Mater. Sci. Eng.*, 2003, **11**, 173–177.

Published on 07 October 2010 on http://pubs.rsc.org | doi:10.1039/C0NR00486C
Downloaded on 17 February 2011

 This journal is © The Royal Society of Chemistry 2011